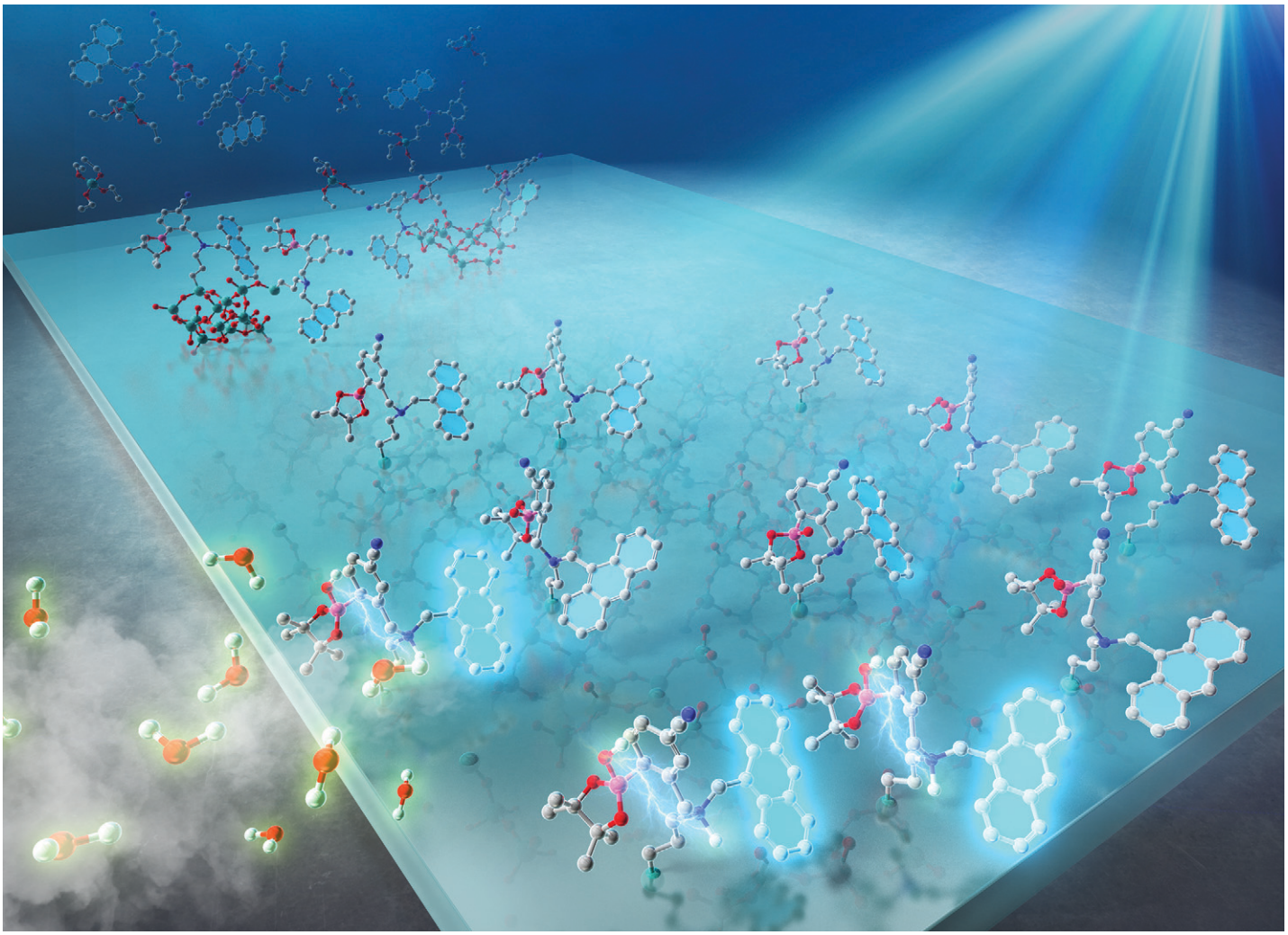

Showcasing research from Professor Yousuke Ooyama's Functional Dye Chemistry laboratory, Applied Chemistry Program, Graduate School of Advanced Science and Engineering, Hiroshima University, Japan.

Anthracene-(aminomethyl)phenylboronic acid ester-immobilized glass substrate as fluorescent sensing materials based on photo-induced electron transfer for detection and visualization of water

We propose that a photo-induced electron transfer (PET)-type fluorescent sensor-immobilized glass substrate is a reversible and reusable functional dye material possessing excellent durability based on a fluorescence off–on switching system not only for visualization and detection of moisture and water droplets but also for constructing fast-response and robust humidity systems, which are widely used in medical, pharmaceutical, cosmetic and industrial fields, as well as for food inspection, environmental quality control monitoring and so on.

As featured in:

See Yousuke Ooyama *et al.*, *Sens. Diagn.*, 2024, **3**, 631.

ROYAL SOCIETY OF CHEMISTRY

rsc.li/sensors

Registered charity number: 207890

Sensors & Diagnostics

PAPER

View Article Online
View Journal | View Issue

Cite this: *Sens. Diagn.*, 2024, **3**, 631

Anthracene-(aminomethyl)phenylboronic acid ester-immobilized glass substrates as fluorescent sensing materials based on photo-induced electron transfer for detection and visualization of water†

Kazuki Tao, Keiichi Imato and Yousuke Ooyama *

As a reversible and reusable fluorescent material possessing excellent durability for detecting and visualizing moisture and water droplets, we have designed and synthesized a PET (photo-induced electron transfer)-type fluorescent monomer **KT-2** composed of anthracene fluorophore-(aminomethyl)-4-cyanophenylboronic acid pinacol ester (AminoMeCNPhenylBPin) with a 3-(triethoxysilyl)propyl group on the amino moiety and achieved preparation of drop-cast **poly(KT-2-*co*-TEOS** or **GPTMS)**silsesquioxane (**SQ**) films on glass substrates *via* the sol–gel reaction of **KT-2** and tetraethoxysilane (TEOS) or (3-glycidyloxypropyl)trimethoxysilane (GPTMS). **KT-2** exhibited enhancement of the fluorescence emission with the increase in water content in various solvents (less polar, polar, protic, and aprotic solvents) due to the formation of the PET inactive (fluorescent) species **KT-2W** by the interaction with water molecules. The detection limit (DL) of **KT-2** for water in the low water content region below 1.0 wt% in the solvents was 0.015–0.020 wt%, indicating that **KT-2** can act as a PET-type fluorescent sensor for a trace amount of water in solvents. Indeed, it was found that the **poly(KT-2-*co*-TEOS** or **GPTMS)SQ** films exhibited a reversible fluorescence off–on switching between the PET active state under a dry process and the PET inactive state under a wet process. Actually, the **poly(KT-2-*co*-TEOS** or **GPTMS)SQ** films initially exhibited a weak blue emission under a dry process but visually apparent blue emission upon exposure to moisture (under a wet process). In particular, the **poly(KT-2-*co*-TEOS)SQ** film displays superior reversible switching performance with a huge change in the fluorescence intensity in the dry–wet process compared with the **poly(KT-2-*co*-GPTMS)SQ** film. This result is attributed to the fact based on the measurements of water contact angles and the roughness on the film surfaces that the **poly(KT-2-*co*-TEOS)SQ** film with a pitted uneven structure has large amounts of **KT-2** units on the surface which make it possible to form the PET inactive **KT-2W** structure by the interaction with water molecules. Herein, we propose that PET-type fluorescent sensor-immobilized glass substrates are one of the most promising and convenient functional dye materials based on a fluorescence off–on switching system for detecting and visualizing moisture and water droplets.

Received 7th October 2023,
Accepted 2nd March 2024

DOI: 10.1039/d3sd00264k

rsc.li/sensors

Introduction

In recent years, there has been increasing interest in the development of fluorescent sensors and their functional materials, including polymers, membranes, and sensor-immobilized substrates for detecting and visualizing water in solids, solutions, and gas or on material surfaces, because such fluorescent sensing systems for water are crucial to environmental and quality control monitoring, industrial processes, food inspection and so on.[1–24] Actually, some kinds of organic fluorescent sensors for water, based on ICT (intramolecular charge transfer),[25–33] ESIPT (excited state intramolecular proton transfer),[34–37] PET (photo-induced electron transfer),[38–52] or solvatochromism have been developed which exhibit photophysical changes in wavelength, intensity, and lifetime of fluorescence emission depending on the water content. Hence, over the last decade and a half, we continued to make much effort to design and develop PET-type fluorescent sensors for water in solvents.[38] As a result, we demonstrated that the PET-type fluorescent

Applied Chemistry Program, Graduate School of Advanced Science and Engineering, Hiroshima University, 1-4-1 Kagamiyama, Higashi-Hiroshima 739-8527, Japan. E-mail: yooyama@hiroshima-u.ac.jp

† Electronic supplementary information (ESI) available. See DOI: https://doi.org/10.1039/d3sd00264k

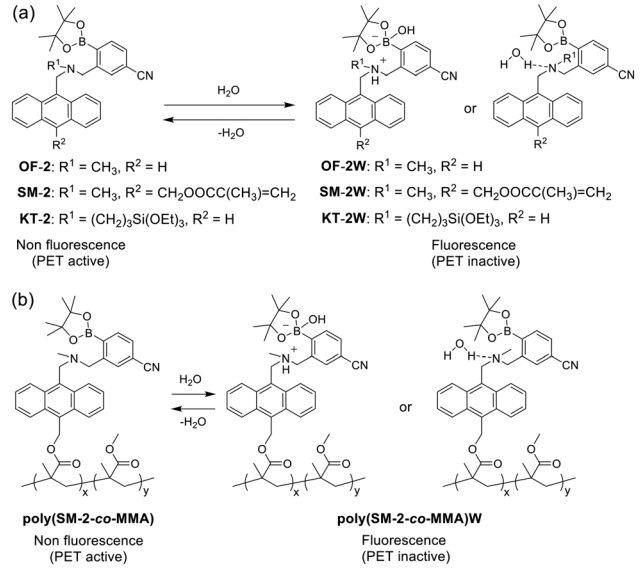

Fig. 1 Mechanisms of PET-type fluorescent sensors (a) **OF-2**, **SM-2** (previous work), **KT-2** (this work), and (b) **poly(SM-2-*co*-MMA)** for detection of water in organic solvents and films.

sensors are based on a fluorescence enhancement (turn-on) system that shows an increase in the fluorescence intensity with the increase in water content in solvents. In particular, it was found that anthracene fluorophore-(aminomethyl)-4-cyanophenylboronic acid pinacol ester (amino-MeCNPhenylBPin) **OF-2** is a highly sensitive PET-type fluorescent sensor for the detection and quantification of a trace amount of water in polar, less polar, protic, and aprotic solvents (Fig. 1a).[42] For **OF-2**, the PET takes place from the nitrogen atom of the amino moiety to the photoexcited anthracene fluorophore in the absence of water, leading to quenching of the fluorescence (in the PET active state). When water is added to the solution of **OF-2**, the nitrogen atom of the amino moiety is protonated or strongly interacts with water molecules to form the PET inactive (fluorescent) species **OF-2W**, and as a result, a drastic enhancement of the fluorescence emission is observed due to the suppression of PET. Indeed, the detection limit (DL) and quantitation limit (QL) of **OF-2** for water in acetonitrile are, respectively, 0.009 wt% and 0.026 wt%, which are equivalent or superior to those of fluorescence quenching systems (turn-off) based on the reported ICT-type[25–33] and ESIPT-type[34–37] fluorescent sensors. Thus, it was demonstrated that the PET method based on the fluorescence enhancement (turn-on) system makes it possible to visualize, detect, and determine a trace amount of water in solvents.

Furthermore, in our previous work, we have designed and developed a PET-type fluorescent monomer **SM-2** composed of methyl methacrylate-substituted anthracene-AminoMeCNPhenylBPin and achieved preparation of **poly(SM-2-*co*-MMA)** by copolymerization of **SM-2** and methyl methacrylate (MMA) (Fig. 1a and b).[51] The DL and QL of **SM-2** for water in acetonitrile were, respectively, 0.009 wt% and 0.028 wt%, which were equivalent to those of **OF-2**. Interestingly, the spin-coated **poly(SM-2-*co*-MMA)** films on a glass substrate produced a reversible fluorescence off–on switching between the PET active state under a dry process and the PET inactive state upon exposure to moisture, which is demonstrated by the fact that the polymer film surface shows moderate hydrophilicity with a water contact angle of *ca.* 70°. Meanwhile, Suzuki *et al.* have reported the preparation of a polymeric dye-immobilized glass plate as a colorimetric sensor material for detecting water content in organic solvents,[53,54] although no information was provided about the fluorescence properties of the functionalized glass plate. Thus, their work inspired us to conceive a PET-type fluorescent monomer with an alkoxysilyl group for creating fluorescent sensor-immobilized glass materials with adequate durability.

Thus, in this work, to develop a reversible and reusable fluorescent material possessing excellent durability for

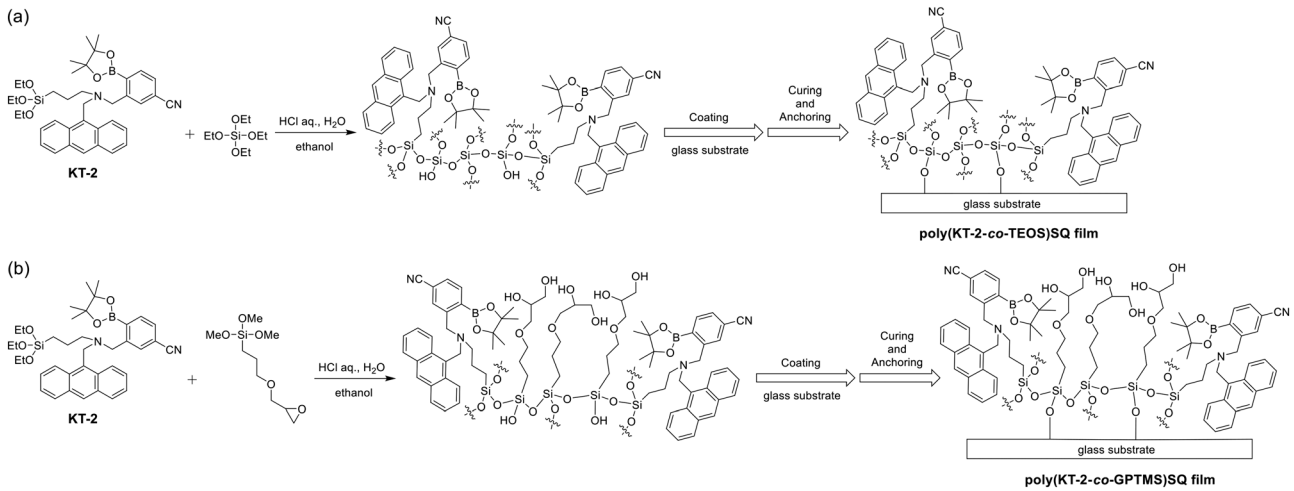

Fig. 2 Preparation of drop-cast (a) **poly(KT-2-*co*-TEOS)** and (b) **poly(KT-2-*co*-GPTMS)**silsesquioxane (**SQ**) films on glass substrates *via* the sol–gel reaction of PET-type fluorescent monomer **KT-2** and tetraethoxysilane (TEOS) or (3-glycidyloxypropyl)trimethoxysilane (GPTMS).

detecting and visualizing moisture and water droplets, we have designed and synthesized a PET (photo-induced electron transfer)-type fluorescent monomer **KT-2** composed of anthracene fluorophore-AminoMeCNPhenylBPin with a 3-(triethoxysilyl)propyl group on the amino moiety and achieved preparation of **poly(KT-2-*co*-TEOS** or **GPTMS)** silsesquioxane (**SQ**) films on glass substrates *via* the sol–gel reaction of **KT-2** and tetraethoxysilane (TEOS) or (3-glycidyloxypropyl)trimethoxysilane (GPTMS) (Fig. 2). It was found that the drop-cast **poly(KT-2-*co*-TEOS** or **GPTMS)SQ** films exhibited a reversible fluorescence off–on switching between the PET active state under a dry process and the PET inactive state under a wet process. Actually, the **poly(KT-2-*co*-TEOS** or **GPTMS)SQ** films initially exhibited a weak blue emission under a dry process but visually apparent blue emission upon exposure to moisture (under a wet process). Herein, we demonstrate that PET-type fluorescent sensor-immobilized glass substrates are one of the most promising and convenient functional dye materials based on a fluorescence off–on switching system for detecting and visualizing moisture and water droplets.

Results and discussion

Synthesis of KT-2

The PET-type fluorescent monomer **KT-2** was synthesized according to a stepwise synthetic protocol (Scheme 1). 9-Anthracenecarboxaldehyde was treated with 3-aminopropyltriethoxysilane to give the intermediate imine, which was then reduced with sodium borohydride to yield **1** (AnTES).[55] The reaction of **1** with 3-(bromomethyl)-4-(4,4,5,5-tetramethyl-1,3,2-dioxaborolan-2-yl)benzonitrile yielded **KT-2**. The characterization of **KT-2** was successfully determined by FT-IR, ^{1}H and ^{13}C NMR measurements, and HRMS analysis.

Optical sensing ability of KT-2 for water in solvents

The optical sensing ability of **KT-2** for water in solvents was investigated by photoabsorption and fluorescence spectral measurements in 1,4-dioxane and THF as less polar solvents, acetonitrile as a polar solvent, and ethanol as a protic solvent containing various concentrations of water (in the water content region below 10 wt%) (Fig. 3). As in the case of **OF-2**,[42] **KT-2** in all four solvents showed a vibronically-structured photoabsorption band originating from the anthracene skeleton in the range of 300 nm to 400 nm and did not undergo appreciable changes in the absorbance and shape upon the addition of water to the solutions (Fig. 3a, c, e and g). The corresponding fluorescence spectra of **KT-2** in the absolute solvents showed a weak and vibronically-structured fluorescence band with a fluorescence maximum wavelength (λ^{fl}_{max}) of around 415 nm in the range of 400 nm to 500 nm, which is ascribable to the

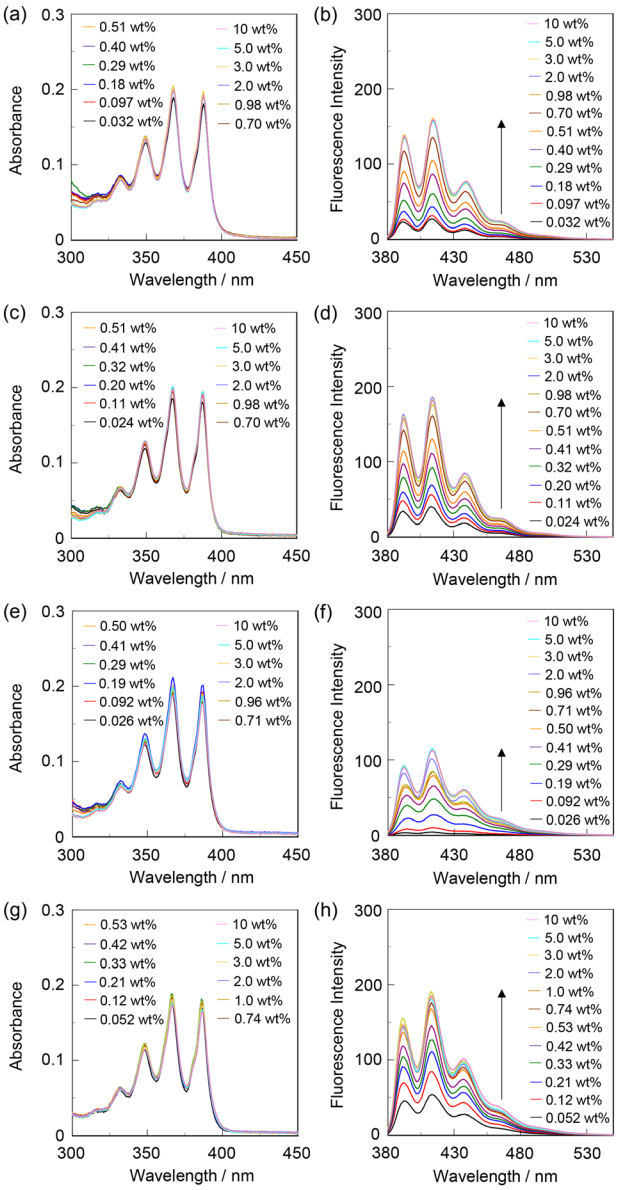

Fig. 3 (a) Photoabsorption and (b) fluorescence spectra (λ^{ex} = 367 nm) of **KT-2** (2.0×10^{-5} M) in 1,4-dioxane containing water (0.032–10 wt%). (c) Photoabsorption and (d) fluorescence spectra (λ^{ex} = 367 nm) of **KT-2** (2.0×10^{-5} M) in THF containing water (0.024–10 wt%). (e) Photoabsorption and (f) fluorescence spectra (λ^{ex} = 367 nm) of **KT-2** (2.0×10^{-5} M) in acetonitrile containing water (0.026–10 wt%). (g) Photoabsorption and (h) fluorescence spectra (λ^{ex} = 367 nm) of **KT-2** (2.0×10^{-5} M) in ethanol containing water (0.052–10 wt%).

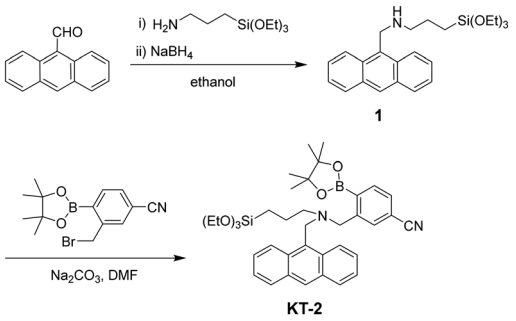

Scheme 1 Synthesis of **KT-2**.

monomer emission originating from the anthracene fluorophore in the PET active state (Fig. 3b, d, f and h). In contrast to the photoabsorption spectra upon the addition of water to the solutions, the fluorescence band increased in the intensity with the increase in the water content in the solution, indicating the formation of the PET inactive (fluorescent) species **KT-2W** by the addition of a water molecule, as in the case of **OF-2** (Fig. 1a). It is worth mentioning that the fluorescence enhancement was saturated in the low water content region below 1.0 wt% in all four solvents. Actually, one can see that the 1,4-dioxane solution of **KT-2** without the addition of water show a weak fluorescence emission but exhibited strong blue fluorescence emission upon the addition of water (Fig. 4a).

In order to confirm the formation of the PET inactive species **KT-2W** by the interaction of **KT-2** with a water molecule, we performed ^{1}H NMR spectral measurements of **KT-2** in THF-d_8 with and without the addition of water (Fig. 5). The ^{1}H NMR spectrum of the **KT-2** solution (with a water content of 0.043 wt%) without the addition of water showed an obvious signal that can be assigned to a single chemical species with the **KT-2** structure. Meanwhile, compared to the ^{1}H NMR spectrum of the **KT-2** solution without the addition of water, some additional signals appeared in both the aliphatic and aromatic regions in the ^{1}H NMR spectrum of the **KT-2** solution with a water content of 1.21 wt% which indicate the existence of other chemical species aside from **KT-2**. Moreover, the ^{1}H NMR spectrum of the **KT-2** solution with a water content of 3.24 wt% can be assigned to a single chemical species which is quite different from the **KT-2** structure; the chemical shifts of the methylene protons H_g next to the phenyl group, the aromatic proton H_l of the phenyl group, and the aromatic proton H_p of the anthracene skeleton showed considerably upfield shifts, while those of the methylene protons H_h next to the anthracene skeleton, the aromatic proton H_m of the phenyl group, and the aromatic proton H_o of the anthracene skeleton showed considerably downfield shifts. Therefore, this result demonstrates that the formation of the PET inactive species **KT-2W** by the interaction with water molecules occurred upon the addition of water to the **KT-2** solution (Fig. 1a), as in the case of **OF-2**.[42]

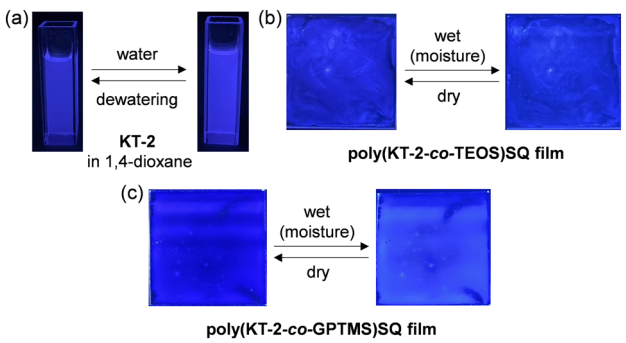

Fig. 4 Photographs (under 365 nm irradiation) of (a) 1,4-dioxane solutions of **KT-2** before and after addition of water and (b) drop-cast **poly(KT-2-*co*-TEOS)SQ** and (c) **poly(KT-2-*co*-GPTMS)SQ** films before and after exposure to moisture.

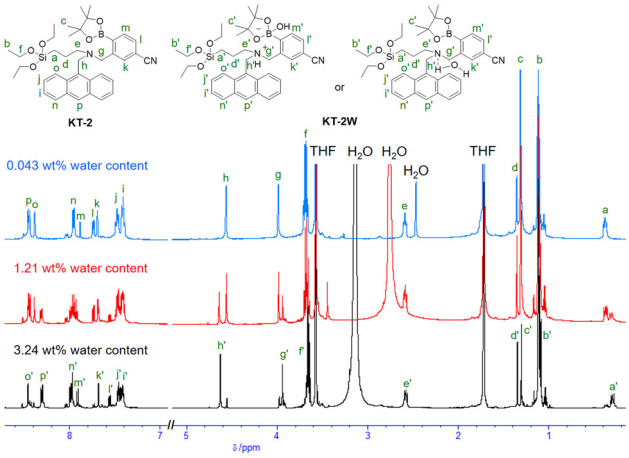

Fig. 5 ^{1}H NMR spectra of **KT-2** (2.0×10^{-2} M) in THF-d_8 with 0.043 wt%, 1.21 wt%, and 3.24 wt% water content.

The sensitivity and accuracy of **KT-2** for the detection of water in solvents were evaluated by the changes in the fluorescence peak intensity at around 415 nm and the plots against the water fraction in solvents (Fig. 6). The plots for **KT-2** demonstrated that the fluorescence peak intensity increased linearly as a function of the water content in the low water content region below 1.0 wt% in all four solvents (Fig. 6a), and thus the fluorescence intensity leveled off when the water content reached *ca.* 1.0 wt% as in the case of **OF-2**.[42] The results of the plots for **KT-2** are as follows:

$$\text{1,4-Dioxane: } F = 171.2[H_2O] + 15.7 \quad (R^2 = 0.990, [H_2O] = 0.032\text{–}0.70 \text{ wt\%}) \tag{1}$$

$$\text{THF: } F = 181.9[H_2O] + 35.1 \quad (R^2 = 0.998, [H_2O] = 0.024\text{–}0.70 \text{ wt\%}) \tag{2}$$

$$\text{Acetonitrile: } F = 164.9[H_2O] - 2.10 \quad (R^2 = 0.993, [H_2O] = 0.026\text{–}0.50 \text{ wt\%}) \tag{3}$$

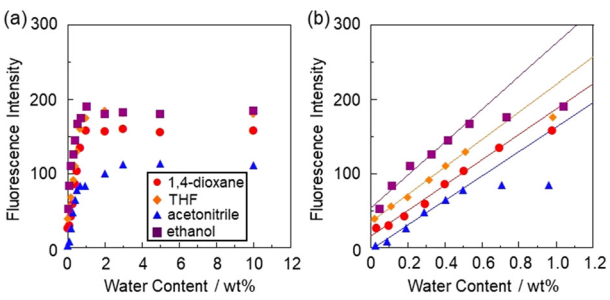

Fig. 6 Fluorescence peak intensity at around 415 nm of **KT-2** (λ^{ex} = 367 nm) as a function of water content below (a) 10 wt% and (b) 1.0 wt% in 1,4-dioxane, THF, acetonitrile, and ethanol.

$$\text{Ethanol: } F = 221.9[H_2O] + 53.2 \quad (R^2 = 0.968, [H_2O] = 0.052\text{–}0.53 \text{ wt\%}) \tag{4}$$

The calibration curves for **KT-2** show good linearity with correlation coefficient (R^2) values of 0.968–0.998. A linear change in fluorescence intensity as a function of water content is one of the factors required for the practical use of a fluorescent sensor. The intercept value (53.2) of the calibration curve for ethanol is higher than those (−2.10–35.1) for 1,4-dioxane, THF, and acetonitrile. It is considered that the enhanced fluorescence of **KT-2** in absolute ethanol is attributed to the suppression of PET by the hydrogen bonding between the hydroxyl group of ethanol and the amino moiety of **KT-2**, as in the case of **OF-2**.[42] It is worth mentioning here that there was a little difference in the m_s values (164–221) for **KT-2** between the four solvents, while the m_s values for **KT-2** were smaller than those (334–390) for **OF-2** (Table 1). The small m_s values for **KT-2** relative to **OF-2** can be attributed to the fact that the flexible 3-(triethoxysilyl) propyl group leads to nonradiative vibrational relaxation of the excited state. Actually, the fluorescence quantum yields (Φ_{fl}) of **OF-2** and **KT-2** in absolute THF were below 3%, but in THF with 1.0 wt% water content, the Φ_{fl} (17%) of **OF-2W** was higher than that (13%) of **KT-2W**. The DLs and QLs of **KT-2** for water in the solvents were determined based on the following equations: DL = $3.3\sigma/m_s$ and QL = $10\sigma/m_s$, where σ is the standard deviation of the blank sample and m_s is the slope of a calibration curve obtained from the plot of the fluorescence peak intensity at around 415 nm *versus* the water fraction in the low water content region below 1.0 wt% (Fig. 6b). The DLs and QLs of **KT-2** for water were, respectively, 0.019 and 0.058 wt% in 1,4-dioxane, 0.018 and 0.055 wt% in THF, 0.020 and 0.060 wt% in acetonitrile, and 0.015 and 0.045 wt% in ethanol, which were inferior to those of **OF-2** because the Φ_{fl} (13%) of **KT-2W** is lower than that (17%) of **OF-2W**. Nevertheless, it was found that anthracene-AminoMeCNPhenylBPin **KT-2** with a 3-(triethoxysilyl)propyl group can act as a PET-type fluorescent sensor for the detection and quantification of a trace amount of water in polar, less polar, protic, and aprotic solvents.

Table 1 DLs and QLs of **OF-2**, **SM-2**, and **KT-2** for water in various organic solvents

Sensor	Solvent	m_s[a]	DL[b]	QL[b]
OF-2 (ref. 42)	1,4-Dioxane	334	0.010 wt%	0.030 wt%
	THF	390	0.008 wt%	0.026 wt%
	Acetonitrile	382	0.009 wt%	0.026 wt%
	Ethanol	362	0.009 wt%	0.027 wt%
SM-2 (ref. 51)	1,4-Dioxane	288	0.011 wt%	0.035 wt%
	THF	326	0.010 wt%	0.030 wt%
	Acetonitrile	355	0.009 wt%	0.028 wt%
	Ethanol	317	0.010 wt%	0.032 wt%
KT-2	1,4-Dioxane	171	0.019 wt%	0.058 wt%
	THF	181	0.018 wt%	0.055 wt%
	Acetonitrile	164	0.020 wt%	0.060 wt%
	Ethanol	221	0.015 wt%	0.045 wt%

[a] Slope of the calibration curve. [b] Detection limit (DL) and quantitation limit (QL) of the sensor for water. DL = $3.3\sigma/m_s$ and QL = $10\sigma/m_s$, where σ is the standard deviation of the blank sample and m_s is the slope of a calibration curve obtained from the plot of the fluorescence peak intensity at around 415–420 nm *versus* the water fraction in the low water content region below 1.0 wt%.

Preparation of poly(KT-2-*co*-TEOS or GPTMS)SQ films and their optical sensing ability for moisture

As reversible and reusable fluorescent materials possessing excellent durability for detecting and visualizing moisture, we prepared **poly(KT-2-*co*-TEOS** or **GPTMS)SQ** films on glass substrates *via* the sol–gel reaction of **KT-2** and TEOS or GPTMS (Fig. 2), and the photoabsorption and fluorescence spectra of the drop-cast **SQ** films before and after exposure to moisture were repeatedly measured several times (Fig. 7). The as-prepared **poly(KT-2-*co*-TEOS)SQ** and **poly(KT-2-*co*-GPTMS)SQ** films in the dry process showed a vibronically-structured photoabsorption band in the range of 300 nm to 400 nm originating from the anthracene skeleton (Fig. 7a and c). The corresponding fluorescence spectra of both the drop-cast **SQ** films in the dry process exhibited a weak and vibronically-structured fluorescence band with a λ^{fl}_{max} of around 420 nm in the range of 400 nm to 500 nm, which is attributed to the monomer emission originating from the anthracene fluorophore in the PET active state (Fig. 7b and d). When both the drop-cast **SQ** films were exposed to moisture (in the wet process), a slight change in the absorbance was observed due to the disturbance of the baselines in the photoabsorption spectra (Fig. 7a and c). On

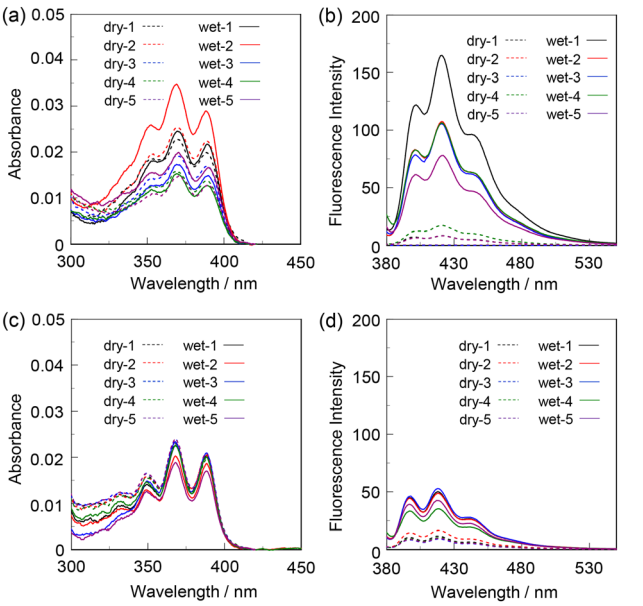

Fig. 7 (a) Photoabsorption and (b) fluorescence spectra (λ^{ex} = 367 nm) of the **poly(KT-2-*co*-TEOS)SQ** film before (in the dry process) and after (in the wet process) exposure to moisture. (c) Photoabsorption and (d) fluorescence spectra (λ^{ex} = 367 nm) of the **poly(KT-2-*co*-GPTMS)SQ** film before (in the dry process) and after (in the wet process) exposure to moisture.

the other hand, the corresponding fluorescence spectra in the wet process showed the enhancement of the vibronically-structured monomer emission band originating from the anthracene fluorophore in the PET inactive state (Fig. 7b and d) but the magnitude of fluorescence enhancement for the **poly(KT-2-*co*-TEOS)SQ** film is larger than that for the **poly(KT-2-*co*-GPTMS)SQ** film. Moreover, when both the drop-cast **SQ** films after exposure to moisture were dried (in the dry process), the photoabsorption and fluorescence spectra recovered the original spectral shapes before exposure to moisture. Accordingly, one can see that both the drop-cast **SQ** films initially exhibit a weak blue emission due to the PET active state under a dry process but visually apparent blue emission due to the PET inactive state upon exposure to moisture (under a wet process) (Fig. 3b and c). Therefore, in order to clarify the difference in the ratio (Fl_{wet}/Fl_{dry}) of the fluorescence intensity as well as the reversibility of the fluorescence intensity in the dry–wet process between the **poly(KT-2-*co*-TEOS)SQ** and **poly(KT-2-*co*-GPTMS)SQ** films, the changes in the fluorescence intensity at λ_{max}^{fl} (*ca.* 420 nm) were plotted against the dry–wet cycle (Fig. 8). It was found that the dry–wet cycles of both the drop-cast **SQ** films showed a good reversible switching of the fluorescence intensity even in the five times dry–wet process. It is worth mentioning here that in the five times dry–wet process, the average of Fl_{wet}/Fl_{dry} for the **poly(KT-2-*co*-TEOS)SQ** film is *ca.* 20, which is significantly higher than that (*ca.* 5) for the **poly(KT-2-*co*-GPTMS)SQ** film.

Thus, in order to investigate the effects of the hydrophilicity and morphology of the drop-cast **SQ** film surfaces on the Fl_{wet}/Fl_{dry} in the dry–wet process, we measured the water contact angles and the roughness on the **poly(KT-2-*co*-TEOS)SQ** and **poly(KT-2-*co*-GPTMS)SQ** film surfaces. The water contact angle (104°) on the **poly(KT-2-*co*-TEOS)SQ** film surface was larger than that (84°) on the **poly(KT-2-*co*-GPTMS)SQ** film surface (Fig. 9), indicating that the **poly(KT-2-*co*-GPTMS)SQ** film is more hydrophilic due to the formation of the diol group by the hydrolysis of the epoxy group in GPTMS (Fig. 2b) than the **poly(KT-2-*co*-TEOS)SQ** film. On the other hand, the 3D images of the drop-cast **SQ** film surfaces obtained using a laser microscope demonstrated that the **poly(KT-2-*co*-TEOS)SQ** film has a pitted uneven surface structure but the **poly(KT-2-*co*-TEOS)SQ** film has a relatively smooth surface (Fig. 10). Indeed, the arithmetic mean roughness (R_a) and the developed interfacial area ratio (Sdr) of the **poly(KT-2-*co*-TEOS)SQ** film surface are evaluated to be *ca.* 10 μm and 219%, respectively, which are much larger than those (8.8 μm and 10.6%) of the **poly(KT-2-*co*-GPTMS)SQ** film surface, suggesting that the **poly(KT-2-*co*-TEOS)SQ** film has large amounts of **KT-2** units on the surface which make it possible to form the PET inactive **KT-2W** structure by the interaction with water molecules, compared to the **poly(KT-2-*co*-GPTMS)SQ** film. Meanwhile, the relatively low hydrophilicity of the **poly(KT-2-*co*-TEOS)SQ** film is likely to be caused by the pitted uneven surface structure with the high R_a value due to the procedure for measuring water contact angles, which is fully understood by the relationship between the surface roughness and the water contact angle based on Wenzel and Cassie–Baxter equations (models).[56–58] Thus, these facts provide the evidence that the **poly(KT-2-*co*-TEOS)SQ** film displays superior reversible switching performance with a huge change in the fluorescence intensity in the dry–wet process compared with the **poly(KT-2-*co*-GPTMS)SQ** film. Consequently, this work demonstrated that PET-type fluorescent sensor-immobilized glass substrates produce a satisfactory reversible fluorescence off–on switching between the PET active state and the PET inactive state during the dry–wet process, and thus are one of the most promising and convenient functional dye materials possessing excellent durability for achieving the visualization and detection of moisture and water droplets.

Experimental

General

IR spectra were recorded using a SHIMADZU IRTracer-100 spectrometer by the ATR method. ^{1}H and ^{13}C NMR spectra were recorded using a Varian-400 or Varian-500 FT NMR spectrometer. High-resolution mass spectral data obtained by ESI were acquired using a Thermo Fisher Scientific LTQ Orbitrap XL. Recycling gel permeation chromatography (GPC) was performed using an RI-detector (GL Science RI 704), a pump (GILSON 307 PUMP), and two columns (Shodex GPC H-2001L). Photoabsorption spectra were observed using a SHIMADZU UV-3600 plus spectrometer. Fluorescence spectra

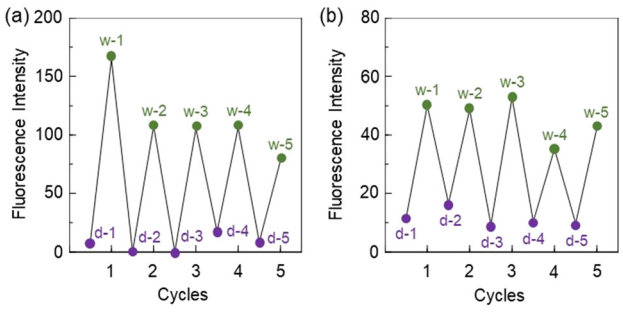

Fig. 8 Reversible switching of fluorescence intensity at around 420 nm of the (a) **poly(KT-2-*co*-TEOS)SQ** film and (b) **poly(KT-2-*co*-GPTMS)SQ** film during the dry–wet process.

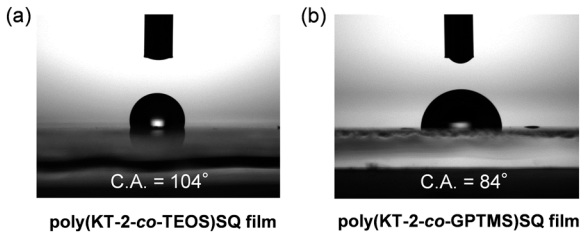

Fig. 9 Water contact angle images of the (a) **poly(KT-2-*co*-TEOS)SQ** film and (b) **poly(KT-2-*co*-GPTMS)SQ** film.

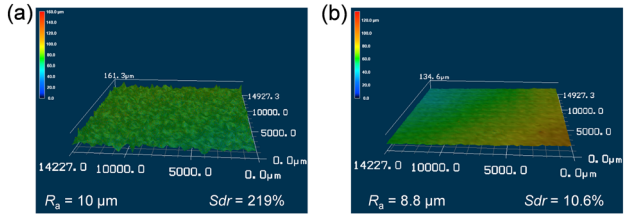

Fig. 10 3D laser microscopy images of the (a) **poly(KT-2-*co*-TEOS)SQ** film and (b) **poly(KT-2-*co*-GPTMS)SQ** film.

were measured using a Hitachi F-4500 spectrometer. The fluorescence quantum yields were determined using a Hamamatsu C9920-01 equipped with a CCD using a calibrated integrating sphere system. The addition of water to 1,4-dioxane, acetonitrile, THF, or ethanol solutions containing **KT-2** was made in terms of weight percent (wt%). The determination of water in solvents was performed with MKC-610 and MKA-610 Karl Fischer moisture titrators (Kyoto Electronics Manufacturing Co., Ltd) based on Karl Fischer coulometric titration for below 1.0 wt% and volumetric titration for 1.0–10 wt%. The contact angle of water was measured using a DMo-602 (KYOWA). The 3D microscopy images of the drop-cast **poly(KT-2-*co*-TEOS)SQ** and **poly(KT-2-*co*-GPTMS)SQ** films were obtained by using a KEYENCE color 3D laser scanning microscope VK-9700, and the arithmetic average roughness (R_a) and the developed interfacial area ratio (Sdr) of the drop-cast **poly(KT-2-*co*-TEOS)SQ** and **poly(KT-2-*co*-GPTMS)SQ** films were evaluated by analysis of the 3D microscopy images.

Synthesis

***N*-(Anthracene-9-ylmethyl)-3-(triethoxysilyl)propan-1-amine (1).** A solution of 9-anthracenecarboxaldehyde (0.50 g, 2.42 mmol) and 3-aminopropyltriethoxysilane (0.624 ml, 2.67 mmol) in ethanol (400 ml) was stirred for 6 h at room temperature under a nitrogen atmosphere. Then, $NaBH_4$ (0.275 g, 7.27 mmol) was added to the solution in an ice bath, followed by stirring for 30 min. After concentrating under reduced pressure, the resulting residue was extracted with water and chloroform. The organic layer was dried over anhydrous $MgSO_4$, filtered, and concentrated. The resulting residue was dissolved in chloroform and subjected to reprecipitation by methanol, and the supernatant solution was concentrated. The crude was dissolved in chloroform, and recycling GPC (chloroform as eluent) was performed to give **1** as a yellow viscous liquid (0.52 g, 52% yield); IR (ATR): $\tilde{\nu}$ = 2972, 2924, 2882, 1624, 1522, 1445, 1389, 1294, 1163, 1099, 1074, 953, 883, 787, 731 cm^{-1}; ^1H NMR (500 MHz, $CDCl_3$, ppm): δ = 0.72 (t, J = 8.3 Hz, 2H), 1.25 (t, J = 7.0 Hz, 9H), 1.72–1.78 (m, 2H), 2.92 (t, J = 7.3 Hz, 2H), 3.84 (q, J = 7.0 Hz, 6H), 4.74 (s, 2H), 7.47 (t, J = 7.5 Hz, 2H), 7.55 (t, J = 7.6 Hz, 2H), 8.01 (d, J = 8.5 Hz, 2H), 8.37 (d, J = 8.9 Hz, 2H), 8.40 (s, 1H); ^{13}C NMR (125, MHz, $CDCl_3$, ppm): δ = 7.78, 18.13, 23.15, 45.37, 53.00, 58.08, 123.94, 124.57, 125.69, 126.80, 128.85, 130.01, 131.28, 131.67; HRMS (ESI): m/z (%): $[M + H]^+$ calcd. for $C_{24}H_{34}NO_3Si$, 412.23025; found 412.23016.

3-(((Anthracene-9-ylmethyl)(3-(triethoxysilyl)propyl)amino) methyl)-4-(4,4,5,5-tetramethyl-1,3,2-dioxaborolan-2-yl) benzonitrile (KT-2). A solution of **1** (1.0 g, 2.43 mmol) and K_2CO_3 (1.03 g, 9.73 mmol) in DMF (20 ml) was stirred for 2 h at room temperature under a nitrogen atmosphere. Then, a solution of 3-(bromomethyl)-4-(4,4,5,5-tetramethyl-1,3,2-dioxaborolan-2-yl)benzonitrile (0.78 g, 2.43 mmol) in DMF was added to the solution, and the mixture was stirred for 16 h at room temperature. After concentrating under reduced pressure, the resulting residue was extracted with water and chloroform. The organic layer was dried over anhydrous $MgSO_4$, filtered, and concentrated. The crude was dissolved in chloroform, and recycling GPC (chloroform as eluent) was performed to give **KT-2** as a yellow viscous liquid (0.53 g, 34% yield); IR (ATR): $\tilde{\nu}$ = 2974, 2926, 2883, 2229, 1605, 1346, 1074, 953, 731, 656 cm^{-1}; ^1H NMR (400 MHz, $CDCl_3$, ppm): δ = 0.45 (t, J = 8.2 Hz, 2H), 1.18 (t, J = 7.0 Hz, 9H), 1.32 (s, 12H), 1.71–1.79 (m, 2H), 2.60 (t, J = 7.4 Hz, 2H), 3.74 (q, J = 7.0 Hz, 6H), 3.92 (s, 2H), 4.55 (s, 2H), 7.35 (d, J = 7.6 Hz, 1H), 7.44 (t, J = 7.3 Hz, 2H), 7.50 (t, J = 7.6 Hz, 2H), 7.62 (s, 1H), 7.68 (d, J = 7.7 Hz, 1H), 7.96 (d, J = 8.3 Hz, 2H), 8.35 (s, 1H), 8.41 (d, J = 8.8 Hz, 2H); ^{13}C NMR (125 MHz, $CDCl_3$, ppm): δ = 8.18, 18.38, 20.25, 24.94, 50.65, 56.56, 58.36, 58.38, 84.21, 113.65, 119.10, 124.86, 125.06, 125.64, 127.53, 128.72, 128.99, 130.30, 131.39, 131.41, 132.49, 135.46, 148.09 (one aromatic carbon signal was not observed owing to overlapping resonances); HRMS (ESI): m/z (%): $[M + H]^+$ calcd. for $C_{38}H_{50}BN_2O_5Si$, 653.35835; found 653.35840.

Preparation of poly(KT-2-*co*-TEOS)SQ and poly(KT-2-*co*-GPTMS)SQ films

The surface of a glass substrate was activated by immersing it in piranha solution for 12 h, then washed with distilled water, and finally dried at 25 °C. A mixture of **KT-2** (1.47 mg, 2.25 μmol), tetraethyl orthosilicate (TEOS; 2.50 g, 12 mmol) or 3-glycidyloxypropyltrimethoxysilane (GPTMS; 2.84 g, 12 mmol), ethanol (7.01 mL, 120 mmol), ultrapure water (0.1 mL, 6 mmol) and 0.1 M HCl aq (3 drops) was stirred at 25 °C for 16 h. For the film preparation, 250 μl of the resulting mixture was dropped on the piranha-treated glass substrate, and then the drop-cast films were dried at 80 °C for 1 h and 120 °C for 16 h. The drop-cast films were washed with THF and ultrapure water, and then dried at 25 °C. The resulting **poly(KT-2-*co*-TEOS)SQ** or **poly(KT-2-*co*-GPTMS)SQ** film was exposed to moisture for 45 s using a humidifier (in the wet process) and then was dried at 80 °C for 45 min (in the dry process) for performing the photoabsorption spectral measurements with a calibrated integrating sphere system and the fluorescence spectral measurements in the wet–dry process.

Conclusions

We have designed and developed a PET (photo-induced electron transfer)-type fluorescent monomer **KT-2** composed of anthracene fluorophore-AminoMeCNPhenylBPin with a 3-(triethoxysilyl)propyl group on the amino moiety and achieved preparation of **poly(KT-2-*co*-TEOS** or **GPTMS)**silsesquioxane (**SQ**) films on glass substrates *via* the sol–gel reaction of **KT-2** and TEOS or GPTMS, as a fluorescent material for detecting and visualizing moisture and water droplets. It was found that the drop-cast **poly(KT-2-*co*-TEOS)SQ** and **poly(KT-2-*co*-GPTMS)SQ** films exhibited a reversible fluorescence off–on switching between the PET active state under a dry process and the PET inactive state under a wet process. Actually, both the drop-cast **SQ** films initially exhibit a weak blue emission under a dry process but visually apparent blue emission upon exposure to moisture (under a wet process). In particular, the **poly(KT-2-*co*-TEOS)SQ** film displays superior reversible switching performance with a huge change in the fluorescence intensity in the dry–wet process, which is attributed to the fact that the **poly(KT-2-*co*-TEOS)SQ** film with a pitted uneven structure has large amounts of **KT-2** units on the surface which make it possible to form the PET inactive **KT-2W** structure by the interaction with water molecules, compared with the **poly(KT-2-*co*-GPTMS)SQ** film. Consequently, this work proposes that PET-type fluorescent sensor-immobilized glass substrates are one of the most promising and convenient functional dye materials possessing excellent durability not only for achieving the visualization and detection of moisture and water droplets but also for constructing a fast-response and robust humidity system which is widely available in medical, pharmaceutical, cosmetic, and industrial fields, food inspection, environmental and quality control monitoring and so on. Meanwhile, the investigation for the optical sensing ability of PET-type fluorescent sensor-immobilized glass substrates under basic and acidic atmospheres are ongoing in our laboratory.

Conflicts of interest

There are no conflicts to declare.

Acknowledgements

This work was supported by Grants-in-Aid for Scientific Research (B) from the Japan Society for the Promotion of Science (JSPS) KAKENHI Grant Number 22H02123 and by The Japan Research Institute of Industrial Science.

Notes and references

1 S. Mishra and A. K. Singh, *Coord. Chem. Rev.*, 2021, **445**, 214063.
2 H. S. Jung, P. Verwilst, W. Y. Kim and J. S. Kim, *Chem. Soc. Rev.*, 2016, **45**, 1242–1256.
3 W. Cheng, Y. Xie, Z. Yang, Y. Sun, M.-Z. Zhang, Y. Ding and W. Zhang, *Anal. Chem.*, 2019, **91**, 5817–5823.
4 L. Liu, Q. Zhang, H. Duan, C. Li and Y. Lu, *Anal. Methods*, 2021, **13**, 3792–3798.
5 T. Maeda and F. Würthner, *Chem. Commun.*, 2015, **51**, 7661–7664.
6 S. Roy, S. Das, A. Ray and P. P. Parui, *New J. Chem.*, 2021, **45**, 4574–4583.
7 P. Kumar, R. Sakla, A. Ghosh and D. A. Jose, *ACS Appl. Mater. Interfaces*, 2017, **9**, 25600–25605.
8 K. Tanaka, K. Nishino, S. Ito, H. Yamane, K. Suenaga, K. Hashimoto and Y. Chujo, *Faraday Discuss.*, 2017, **196**, 31–42.
9 H. Mori, K. Nishino, K. Wada, Y. Morisaki, K. Tanaka and Y. Chujo, *Mater. Chem. Front.*, 2018, **2**, 573–579.
10 K. Nishino, H. Yamamoto, J. Ochi, K. Tanaka and Y. Chujo, *Chem. – Asian J.*, 2019, **14**, 1577–1581.
11 Y.-C. Liu, G.-D. Lu, J.-H. Zhou, J.-W. Rong, H.-Y. Liu and H.-Y. Wang, *RSC Adv.*, 2022, **12**, 7405–7412.
12 W.-E. Lee, Y.-J. Jin, L.-S. Park and G. Kwak, *Adv. Mater.*, 2012, **24**, 5604–5609.
13 D.-C. Han, Y.-J. Jin, J.-H. Lee, S.-I. Kim, H.-J. Kim, K.-H. Song and G. Kwak, *Macromol. Chem. Phys.*, 2014, **215**, 1068–1076.
14 Q. Deng, Y. Li, J. Wu, Y. Liu, G. Fang, S. Wang and Y. Zhang, *Chem. Commun.*, 2012, **48**, 3009–3011.
15 J. Lee, M. Pyo, S. Lee, J. Kim, M. Ra, W.-Y. Kim, B. J. Park, C. W. Lee and J.-M. Kim, *Nat. Commun.*, 2014, **5**, 3736.
16 K.-I. Hong, A. H. Yang, Y. Kim, M. Ranathunga, U. Kim, C. Joo and W.-D. Jang, *Sens. Actuators, B*, 2023, **387**, 133756.
17 Y. Sun, L. Wei, S. Zhu, P. Jin, C. He, Q. He, C. Yang and W. Wu, *Sens. Actuators, B*, 2023, **387**, 133764.
18 P. P. Dash, P. Mohanty, R. Behura, S. Behera, P. Singla, S. C. Sahoo, S. K. Sahoo and B. R. Jali, *J. Photochem. Photobiol., A*, 2023, **440**, 114650.
19 R. Abhijnakrishna, N. Vijay and S. Velmathi, *New J. Chem.*, 2022, **46**, 17903–17911.
20 A. Tigreros, M. Macías and J. Portilla, *ChemPhotoChem*, 2022, **6**, e202200133.
21 L. Ding, Z. Zhang, X. Li and J. Su, *Chem. Commun.*, 2013, **49**, 7319–7321.
22 M. Turemis, D. Zappi, M. T. Giardia, G. Basile, A. Ramanaviciene, Al. Kapralovs, A. Ramanavicius and R. Viter, *Talanta*, 2020, **211**, 120658.
23 R. Viter, K. Kunene, P. Genys, D. Jevdokimovs, D. Erts, A. Sutka, K. Bisetty, A. Viksna, A. Ramanaviciene and A. Ramanavicius, *Macromol. Chem. Phys.*, 2020, **221**, 1900232.
24 R. Viter, M. Savchuk, N. Starodub, Z. Balevicius, S. Tumenas, A. Ramanaviciene, D. Jevdokimovs, D. Erts, I. Iatsunskyi and A. Ramanavicius, *Sens. Actuators, B*, 2019, **285**, 601–606.
25 I. M. Resta and F. Galindo, *Dyes Pigm.*, 2022, **197**, 109908.
26 Z. Zhao, Q. Hu, W. Liu, X. Xiong, Z. Wang and H. Wang, *Dyes Pigm.*, 2023, **213**, 111186.
27 Z. Li, Q. Yang, R. Chang, G. Ma, M. Chen and W. Zhang, *Dyes Pigm.*, 2011, **88**, 307–314.
28 S. Tsumura, T. Enoki and Y. Ooyama, *Chem. Commun.*, 2018, **54**, 10144–10147.

29 T. Enoki and Y. Ooyama, *Dalton Trans.*, 2019, **48**, 2086–2092.
30 K. Imato, T. Enoki and Y. Ooyama, *RSC Adv.*, 2019, **9**, 31466–31473.
31 C.-G. Niu, P.-Z. Qin, G.-M. Zeng, X.-Q. Gui and A.-L. Guan, *Anal. Bioanal. Chem.*, 2007, **387**, 1067–1074.
32 Z.-Z. Li, C.-G. Niu, G.-M. Zeng and P.-Z. Qin, *Chem. Lett.*, 2009, **38**, 698–699.
33 C.-G. Niu, A.-L. Guan, G.-M. Zeng, Y.-G. Liu and Z.-W. Li, Fluorescence water sensor based on covalent immobilization of chalcone derivative, *Anal. Chim. Acta*, 2006, **577**, 264–270.
34 W. Liu, Y. Wang, W. Jin, G. Shen and R. Yu, *Anal. Chim. Acta*, 1999, **383**, 299–307.
35 J. S. Kim, M. G. Choi, Y. Huh, M. H. Kim, S. H. Kim, S. Y. Wang and S.-K. Chang, *Bull. Korean Chem. Soc.*, 2006, **27**, 2058–2060.
36 H. Mishra, V. Misra, M. S. Mehata, T. C. Pant and H. B. Tripathi, *J. Phys. Chem. A*, 2004, **108**, 2346–2352.
37 A. C. Kumar and A. K. Mishra, *Talanta*, 2007, **71**, 2003–2006.
38 Y. Ooyama, *Sustainable and Functional Redox Chemistry*, ed. S. Inagi, The Royal Society of Chemistry, Cambridge, UK, 2022, ch. 13, pp. 300–330.
39 Y. Ooyama, M. Sumomogi, T. Nagano, K. Kushimoto, K. Komaguchi, I. Imae and Y. Harima, *Org. Biomol. Chem.*, 2011, **9**, 1314–1316.
40 Y. Ooyama, A. Matsugasako, K. Oka, T. Nagano, M. Sumomogi, K. Komaguchi, I. Imae and Y. Harima, *Chem. Commun.*, 2011, **47**, 4448–4450.
41 Y. Ooyama, A. Matsugasako, Y. Hagiwara, J. Ohshita and Y. Harima, *RSC Adv.*, 2012, **2**, 7666–7668.
42 Y. Ooyama, K. Furue, K. Uenaka and J. Ohshita, *RSC Adv.*, 2014, **4**, 25330–25333.
43 Y. Ooyama, M. Hato, T. Enoki, S. Aoyama, K. Furue, N. Tsunoji and J. Ohshita, *New J. Chem.*, 2016, **40**, 7278–7281.
44 Y. Ooyama, R. Sagisaka, T. Enoki, N. Tsunoji and J. Ohshita, *New J. Chem.*, 2018, **42**, 13339–13350.
45 D. Jinbo, K. Imato and Y. Ooyama, *RSC Adv.*, 2019, **9**, 15335–15340.
46 D. Jinbo, K. Ohira, K. Imato and Y. Ooyama, *Mater. Adv.*, 2020, **1**, 354–362.
47 Y. Mise, K. Imato, T. Ogi, N. Tsunoji and Y. Ooyama, *New J. Chem.*, 2021, **45**, 4164–4173.
48 T. Fumoto, S. Miho, Y. Mise, K. Imato and Y. Ooyama, *RSC Adv.*, 2021, **11**, 17046–17050.
49 S. Miho, T. Fumoto, Y. Mise, K. Imato, S. Akiyama, M. Ishida and Y. Ooyama, *Mater. Adv.*, 2021, **2**, 7662–7670.
50 E. Nishimoto, Y. Mise, T. Fumoto, S. Miho, N. Tsunoji, K. Imato and Y. Ooyama, *New J. Chem.*, 2022, **46**, 12474–12481.
51 S. Miho, K. Imato and Y. Ooyama, *RSC Adv.*, 2022, **12**, 25687–25696.
52 T. Fumoto, K. Imato and Y. Ooyama, *New J. Chem.*, 2022, **46**, 21037–21046.
53 H. Hisamoto, Y. Manabe, H. Yanai, H. Tohma, T. Yamada and K. Suzuki, *Anal. Chem.*, 1988, **73**, 1255–1261.
54 D. Citterio, K. Minamihashi, Y. Kuniyoshi, H. Hisamoto, S. Sasaki and K. Suzuki, *Anal. Chem.*, 2001, **73**, 5339–5345.
55 A. B. Descalzo, M. D. Marcos, R. Martínez-Máñez, J. Soto, D. Beltrán and P. Amorós, *J. Mater. Chem.*, 2005, **15**, 2721–2731.
56 A. B. D. Cassie, *Discuss. Faraday Soc.*, 1948, **3**, 11–16.
57 R. N. Wenzel, *J. Phys. Chem.*, 1949, **53**, 1466–1467.
58 A. B. D. Cassie and S. Baxter, *Trans. Faraday Soc.*, 1944, **40**, 546–551.